CHINESE OPTICS LETTERS

Vol. 21, No. 12 | December 2023

Speckle-based interrogation system for quasi-distributed weak fiber Bragg gratings

Jinchao Tao (陶缙超)[1], Qin Liang (梁 芹)[1], Yue Li (李 玥)[1], Yanlong Meng (孟彦龙)[1], Yanqing Qiu (裘燕青)[1], Pengwei Zhou (周鹏威)[1], Chunliu Zhao (赵春柳)[1], Juan Kang (康 娟)[1], Xianchao Zhang (张先超)[2], Zhiguo Jiang (蒋治国)[2], Le Wang (王 乐)[1], and Yi Li (李 裔)[1*]

[1] College of Optical and Electronic Technology, China Jiliang University, Hangzhou 310018, China

[2] Key Laboratory of Medical Electronics and Digital Health of Zhejiang Province, Jiaxing University, Jiaxing 314001, China

*Corresponding author: yli@cjlu.edu.cn

Received May 17, 2023 | Accepted July 14, 2023 | Posted Online December 8, 2023

A simple quasi-distributed fiber sensing interrogation system based on random speckles is proposed for weak fiber Bragg gratings (WFBGs) in this work. Without using tunable lasers or spectrometers, a piece of multimode fiber is applied to interrogate the WFBGs relying on the wavelength sensitivity of speckles. Instead of the CCD sensor, an InGaAs quadrant detector serves as the receiver to capture the fast-changing speckle patterns. A supervised deep learning algorithm of the multilayer perceptron architecture is implemented to process speckle data and to interrogate temperature changes or dynamic strains. The proposed demodulation system is experimentally demonstrated for WFBGs with 0.1% reflectivity. The experimental results demonstrate that the new system is capable of measuring temperature change with an accuracy of 1°C and achieving dynamic frequency of 100 Hz. This speckle-based interrogation system paves a new way for distributed WFBGs sensing with a simple design.

Keywords: weak fiber Bragg gratings; random speckles; deep learning; time-division-multiplexing.
DOI: 10.3788/COL202321.121601

1. Introduction

Optical fiber Bragg gratings (FBGs) have been widely used in the fields of structural health monitoring, petrochemical industry, subsurface deformation monitoring, and force monitoring in biomedical devices for the advantages of compactness, passivity, electro-magnetic resistance, in particular, excellent large-scale multiplexing capacity[1–4]. The intrinsic capability of measuring several parameters, such as temperature, strain, vibration, and many others, is provided by FBG thanks to its spectral shift as a function of these parameters. In recent years, weak FBGs (WFBGs) have drawn immense interest in applications where dense sensing points are required because of their weak reflectivity, which greatly increases the multiplexing capacity and scale of the sensor array[5–7].

The multiplexing techniques mainly include wavelength-division-multiplexing (WDM), time-division-multiplexing (TDM), optical frequency domain reflectometry (OFDR), code-division multiple-access (CDMA), and the hybrid multiplexing using two or three of the methods stated above[8–11]. For the WDM method, the total number of FBGs is determined by the bandwidth of the available optical source, which is often less than 100 nm, and the multiplexing capacity is limited to a few dozens. OFDR operates in the frequency domain, and the FBG positions can be mapped into different heterodyne frequencies using a linear sweep laser. Childers *et al.* experimentally multiplexed 3000 FBGs in four 8 m optical fibers based on an OFDR system. However, this technique is restricted on a relatively short sensing range and polarization fading[12]. Besides, Zhou *et al.* reported a demodulation method based on microwave photonics and chromatic dispersion, with a high demodulation speed of 40 kHz. With the help of the dispersion compensation fiber (DCF), the wavelength shifts of WFBGs are converted to the change of the beat frequencies[13]. Several other types of FBG demodulation methods have been demonstrated in the form of TDM as well[14–17]. The reflection spectra of FBGs can be resolved by scanning hundreds of wavelengths. Nevertheless, limited by the long establishment time of the reflection spectrum, it usually takes a few minutes to complete one round of interrogation[18]. On the other hand, the reflection spectrum can be obtained by a spectrometer consisting of diffraction grating and CCD line[19]. However, this TDM-based method can only demodulate the FBGs one by one, which obviously will slow down the demodulation as the sensing distance increases. Chromatic-dispersion-induced wavelength-to-time mapping was also utilized for high-speed wavelength demodulation,

where the dispersive unit introduces a detectable time delay as a function of the FBG central wavelength shift. A high sampling rate of 40 GS/s was used to catch the marginal time difference between two reflected pulses[20].

Recently, it has been realized that tracking changes of speckle, which is the granular interference pattern produced when light propagates through a random medium, allows highly resolved wavelength measurement[21,22]. A wavelength precision of two attometers was achieved by using a deep learning algorithm to extract the spectral features from speckle patterns[23]. Moreover, the backscattered speckle pattern formed in a multimode fiber (MMF) was used to interrogate a linear strain response with a dynamic range of 74 dB at 1 kHz[24].

In this Letter, we proposed a simple quasi-distributed fiber interrogation system for WFBGs. The measurement of temperature and dynamic strain can be achieved by measuring the speckles generated from a section of MMF, instead of using the tunable laser, tunable filter, or spectrometer required in traditional demodulation methods. Instead of the CCD sensor, an InGaAs quadrant detector (QD) served as the receiver to capture the fast-changing speckle patterns. Thus, the proposed demodulation system can measure all the WFBGs of the sensing link with only one pulse. A multilayer perceptron (MLP) architecture was proposed to process the acquired speckle data. As a result, a low-cost, high-speed, and simple system was realized for WFBGs demodulation in this work.

2. Experiments and Methods

The schematic configuration of the proposed speckle-based WFBGs interrogation system is shown in Fig. 1. The system consists of a light source, a fiber sensing link, an MMF as the light scattering media, and a detection subsystem. Light from a broadband amplified spontaneous emission (ASE, MFAS-Er-1550-M) was filtered by a 2 nm bandwidth optical filter (based on an FBG) with a center wavelength of 1530.5 nm. The continuous-wave (CW) light was modulated into nanosecond pulses by a semiconductor optical amplifier (SOA, Kamelian OPB-12-15-N-C-FA). Considering the bandwidth of the used InGaAs QD (Hamamatsu G6849), the pulses had a temporal width of 30 ns, and the pulse light was then amplified by an erbium-doped fiber amplifier (EDFA) with peak power up to 1 W. Note that the pulse width was selected to be less than the time interval between two adjacent gratings to avoid signal overlap. Different WFBGs can be identified by their different time delays from the reflection signal. Then, the pulse light was launched into the sensing link of identical WFBGs by a circulator.

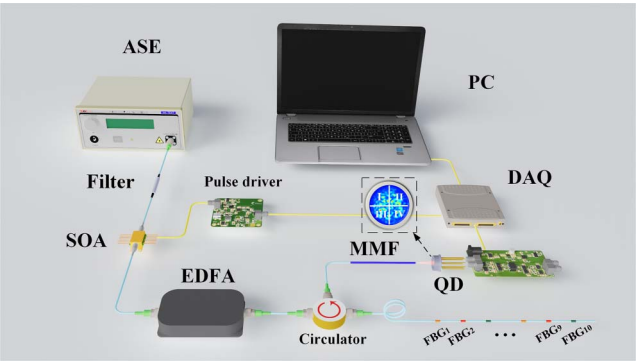

Fig. 1. Schematic configuration of the speckle-based WFBGs interrogation system. The inset graph shows four quadratic photosensitive areas of the QD.

The injected pulse light was reflected by each WFBG and produced a pulse train, in which the central wavelength of the pulse is determined by the local environment. The pulse train exited port 3 of the circulator and then entered a 6 m long MMF (Nufern MM-S105/125-22A). It has 105 μm diameter cores (NA = 0.22), which serve as the random scattering media. Note that the MMF was coiled on a spool and fixed by glue for mechanical stability. Then, the speckle patterns generated at the output of the MMF were divided into four parts, as shown in the inset graph of Fig. 1, and captured by a QD with the bandwidth of 30 MHz. A series of QD data were finally acquired by a data acquisition card (DAQ, ART Technology PCIe8586M) at a sampling rate of 100 MS/s.

When the reflection light injects into the MMF, the electric field at the end of the MMF can be expressed by adapting the standard one-dimensional impulse response model[25,26]:

$$E(x,y,\lambda,t,L) = \sum_{m}^{M}\sum_{n}^{N} R_n(\lambda)A_m\psi_m(x,y)\exp\{-i[\beta_m(\lambda)L - wt + \varphi_m]\} \times \mathrm{rect}\left(\frac{t-\tau_n}{w}\right), \quad (1)$$

where $R_n(\lambda)$ and τ_n are the spectral reflectivity and the delay time of the nth FBG, L is the length of the MMF, and w is the pulse width of the incident light. A_m and φ_m are the amplitude and the initial phase of the mth mode, which has the spatial profile ψ_m and the propagation constant β_m. As the local environment changes, the wavelength shift of the FBGs modifies the propagation constant, causing the guided modes to accumulate different phase delays, thereby changing the speckle pattern[21,27].

3. Results and Discussion

In order to validate the speckle changes with the wavelength shifts of the WFBG, we recorded the speckle patterns with an InGaAs camera (Hamamastu, C10633) and the corresponding reflection spectrum by an optical spectrum analyzer (OSA, Yokogawa AQ6370) with the resolution of 0.02 nm. Figures 2(a) and 2(b) show four speckle patterns and their corresponding reflection spectrum at the temperatures of 20°C, 21°C, 22°C, and 30°C, respectively. It can be seen that the speckle patterns appear in different profiles and intensity distributions at different temperatures. The larger the temperature changes, the more differences between the speckle patterns emerge. The measured

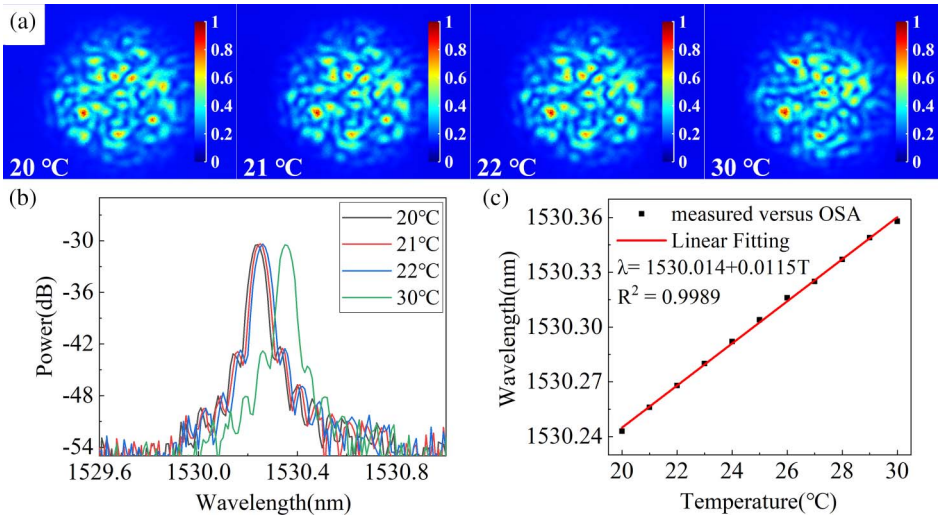

Fig. 2. (a) and (b) Speckle patterns and their corresponding reflection spectrum at the temperatures of 20°C, 21°C, 22°C, and 30°C, respectively. (c) WFBG central wavelength as a function of temperature.

peak wavelength of the WFBG under different temperatures is illustrated in Fig. 2(c), with the temperature sensitivity of 11.5 pm/°C.

To investigate the performance of the proposed interrogation system, 10 WFBGs with the identical central wavelength of 1530.30 nm and an equal separation of 4 m were written on a single-mode optical fiber (SMF-28e) in series. The central wavelengths of reflected light from each WFBG are quite uniform when the local environment such as temperature and strain is stable. Besides, all the WFBGs have a uniform peak reflectivity of 0.1% (−30 dB). Figure 3 shows the whole trace of four measurement channels corresponding to the QD of the WFBG (inset of Fig. 1). The speckle pattern was equally divided into four parts, as shown in the inset graph of Fig. 1. The QD data can be regarded as being significantly compressed compared with the entire speckle images.

In the following experiment, we placed WFBG#9 of the sensing link in the temperature control chamber with a temperature

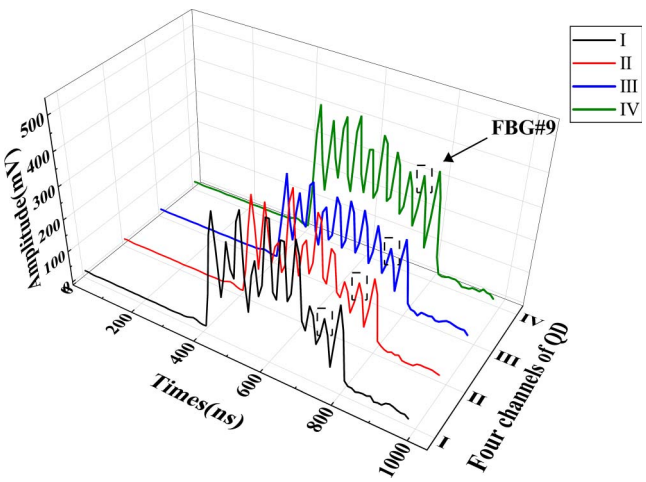

Fig. 3. Acquired four QD data traces of the WFBGs.

controlling precision of 0.1°C, setting the temperature range from 15°C to 44°C. The QD data at different temperatures were recorded every 1°C step. Figure 4(a) shows the original acquired QD data, where I, II, III, and IV correspond to the quadrant receiving area of the QD. When the temperature increased, the QD data changed randomly due to the intrinsic randomness of the speckle distribution. To test the system's stability, the temperature measurements of WFBG#9 at 15°C were repeated for 50 pulses under the same test environment, as shown in Fig. 4(b). It should be noted that the QD intensities were up and down with the same direction, while the data fluctuations were mainly caused by the pulse intensity variation itself.

To interrogate the wavelength dependence of the speckle data, a supervised deep learning algorithm based on the MLP architecture[28] was implemented in this study. The MLP is a data-driven deep learning algorithm that can learn features from high-dimensional data and is used to map speckle data to temperatures or central wavelengths. The schematic diagram is shown in Fig. 5. Here, the input was a series of quadrant data including temperature changes. The MLP consisted of seven hidden layers, each containing 100, 200, 400, 800, 400, 200, and 100 nodes, respectively. The output of each hidden layer was activated by the rectified linear unit (ReLU). The output layer has n neurons with a Softmax activation function to convert it into a probability distribution and gives corresponding classifications, in which n denotes the number of temperature classes. The loss function optimized in this classification network was the standard square error (MSE). An Adam optimizer[29] with a learning rate of 10^{-3} decayed by 50% every 300 epochs. All the codes were conducted using PyTorch.

In the following, we presented the capabilities of MLP to extract temperature-related features from QD data. We varied the temperature by 1°C steps over a range of 30°C. Each data point is represented as a five-dimensional vector whose first element is the temperature label (output), and the remaining

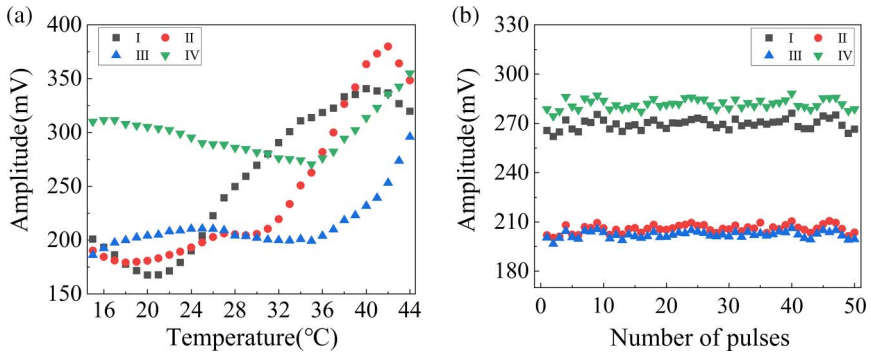

Fig. 4. (a) Original QD data of FBG#9, with I, II, III, and IV corresponding to the quadrant channels. (b) Repeated measurements of FBG#9 at 15°C for 50 pulses.

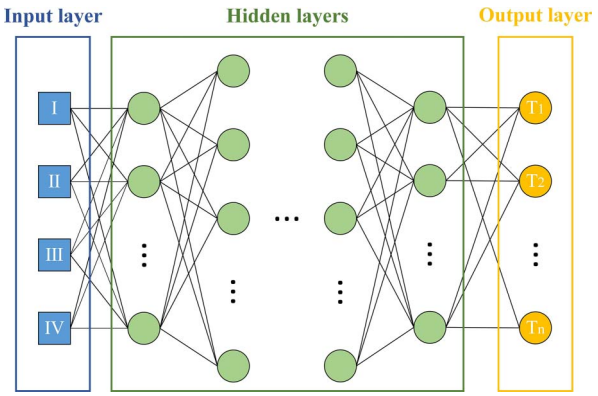

Fig. 5. Schematic diagram of the MLP architecture used in this work.

four elements are the QD data (input). The intensity values in each QD data were normalized between 0 and 1. The complete dataset consisted of 3000 (30 × 100) data, which were randomly divided into training, validation, and test subsets by fractions of 80%, 10%, and 10%, respectively. The training and validation subsets were used to train and cross-validate the fine-tuned hyperparameters such as the learning rate and the batch size, while the testing subset was reserved for evaluation. To calibrate the MLP, the training was performed using every data in the training set and implemented in Python over Nvidia RTX 3060Ti. During training, mini-batches of QD data passed forward through the MLP, which were randomly sampled from the training subset, and the error was minimized by adjusting the network's weights following the standard backpropagation. The loss and the prediction accuracy on the training and validation subsets were monitored after every epoch. This process was repeated until the loss converged to a minimum value, taking approximately 5 min. Figure 6(a) shows the training and validation losses of the MLP during the training epochs, which drop dramatically at the beginning, then approach zero. In order to evaluate the trained MLP, the untrained QD data in the test subset were passed through the network to predict the corresponding temperatures, and the single algorithm runtime was about 5 μs. Moreover, the classification accuracy of test subset by MLP led to 100% measurement accuracy. To visualize the results, we calculated the confusion matrix using the test subset, shown in Fig. 6(b), and it is clear that the resolution of the proposed system is 1°C. Therefore, the trained MLP can extract the features only caused by temperature changes and resist the fluctuations of the light pulse intensity. Furthermore, the temperature was tuned in the step of 0.5°C over a range of 30°C under the same experimental setup. The accuracies of the training subset and validation subset were 92.8% and 94%, respectively.

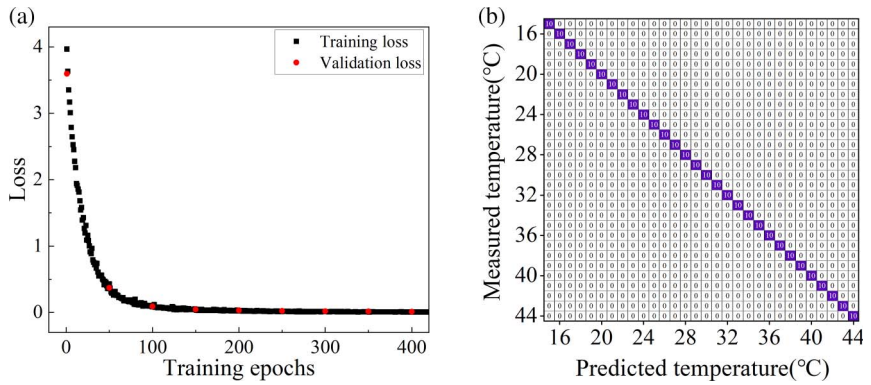

Fig. 6. (a) Training and validation loss reduced during the training epochs. (b) Confusion matrix for the output of the MLP.

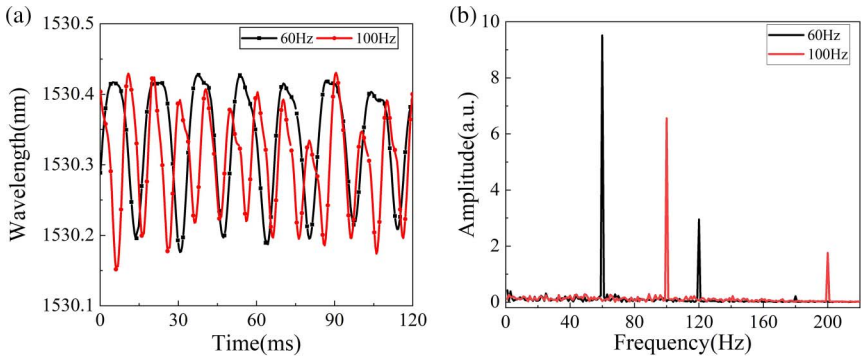

Fig. 7. Demodulation results of the dynamic signal at 60 Hz and 100 Hz: (a) the time domain diagram, (b) the corresponding frequency spectrum.

Benefiting from the high-speed readout of the QD, the feasibility of vibration measurement was proven by the proposed interrogator in the following experiment. A speaker was used as the vibration source to generate dynamic strain acting on the last WFBG in the sensing link. The data were captured by the DAQ, synchronizing with the input pulse light. A series of QD data caused by vibration signals were passed through the trained MLP. Then, we can obtain the corresponding fluctuation of the central wavelength, based on the function of temperature–wavelength [as shown in Fig. 2(c)]. Figure 7(a) shows the wavelength variance of WFBGs in the time domain at 60 Hz and 100 Hz. Figure 7(b) presents the corresponding frequency spectrum intensity by making fast Fourier transform (FFT). Moreover, the high-order harmonics can be observed in Fig. 7(b), which may come from the sinusoidal driving signal or the nonlinear features of speckles.

4. Conclusions

In summary, we experimentally demonstrated a simple quasi-distributed WFBGs interrogation system based on random speckles. In the random scattering media, wavelength shifts of WFBGs are converted to intensity and profile change of speckle patterns. A QD was employed as the speckle patterns receiver, which has a high responding bandwidth compared to the traditional CCD. Although the data were greatly compressed by the QD, the wavelengths of cascade WFBGs could still be demodulated with the help of the MLP. The experiment results showed that the proposed system can realize the wavelength demodulation of WBFGs with 0.1% reflectivity with 4 m spatial interval and the temperature measurement from 15°C to 44°C with an accuracy of 1°C (~11.5 pm). Besides, the measurement of the dynamic stain up to 100 Hz was demonstrated. In contrast to traditional demodulation methods using a tunable laser, tunable filter, or spectrometer, the proposed method exhibits advantages such as low cost and high measurement speed, which greatly simplifies the research for WFBGs interrogation. Only one pulse light can measure the strain/temperature-induced changes in the reflectance of all FBGs, and the limitation of this system is just the round trip time in the fiber. It is believed that the speckle-based interrogation system paves a new way for quasi-distributed sensing with a simple design.

Acknowledgement

This work was supported by the National Key Research and Development Program of China (No. 2021YFC3340400), Key Laboratory of Medical Electronics and Digital Health of Zhejiang Province (No. MEDH202209), Natural Science Foundation of Zhejiang Province (No. LY22F050004), and Zhejiang Xinmiao Talents Program (No. 2022R409043).

References

1. Y. Zhang, G. Keiser, C. Marzinsky, A. M. Schilowitz, L. Song, and A. B. Herhold, "Applications of optical fiber sensors in the oil refining and petrochemical industries," in *SENSORS* (2011), p. 246.
2. S. Liu, B. Shi, K. Gu, C. Zhang, J. He, J. Wu, and G. Wei, "Fiber-optic wireless sensor network using ultra-weak fiber Bragg gratings for vertical subsurface deformation monitoring," Nat. Hazards **109**, 2557 (2021).
3. M. S. Milczewski, J. C. C. Da Silva, C. Martelli, L. Grabarski, I. Abe, and H. J. Kalinowski, "Force monitoring in a maxilla model and dentition using optical fiber Bragg gratings," Sensors **12**, 11957 (2012).
4. J. Leng and A. Asundi, "Structural health monitoring of smart composite materials by using EFPI and FBG sensors," Sens. Actuator A Phys. **103**, 330 (2003).
5. A. L. Ricchiuti, J. Hervás, D. Barrera, S. Sales, and J. Capmany, "Microwave photonics filtering technique for interrogating a very-weak fiber Bragg grating cascade sensor," IEEE Photonics J. **6**, 5501410 (2014).
6. W. Liu, Z. Guan, G. Liu, C. Yan, and S. He, "Optical low-coherence reflectometry for a distributed sensor array of fiber Bragg gratings," Sens. Actuator A Phys. **144**, 64 (2008).
7. L. Xia, R. Cheng, W. Li, and D. Liu, "Identical FBG-based quasi-distributed sensing by monitoring the microwave responses," IEEE Photon. Technol. Lett. **27**, 323 (2014).
8. Z. Luo, H. Wen, H. Guo, and M. Yang, "A time-and wavelength-division multiplexing sensor network with ultra-weak fiber Bragg gratings," Opt. Express **21**, 22799 (2013).
9. K. Yüksel, P. Mégret, and M. Wuilpart, "A quasi-distributed temperature sensor interrogated by optical frequency-domain reflectometer," Meas. Sci. Technol. **22**, 115204 (2011).
10. K. Koo, A. Tveten, and S. Vohra, "Dense wavelength division multiplexing of fibre Bragg grating sensors using CDMA," Electron. Lett. **35**, 165 (1999).

11. M. Götten, S. Lochmann, A. Ahrens, E. Lindner, and J. Van Roosbroeck, "2000 serial FBG sensors interrogated with a hybrid CDM-WDM scheme," J. Lightwave Technol. **38**, 2493 (2020).
12. B. A. Childers, M. E. Froggatt, S. G. Allison, T. C. Moore, Sr., D. A. Hare, C. F. Batten, and D. C. Jegley, "Use of 3000 Bragg grating strain sensors distributed on four 8-m optical fibers during static load tests of a composite structure," Proc. SPIE **4332**, 133 (2001).
13. L. Zhou, Z. Li, N. Xiang, and X. Bao, "High-speed demodulation of weak fiber Bragg gratings based on microwave photonics and chromatic dispersion," Opt. Lett. **43**, 2430 (2018).
14. P. Han, Z. Li, L. Chen, and X. Bao, "A high-speed distributed ultra-weak FBG sensing system with high resolution," IEEE Photon. Technol. Lett. **29**, 1249 (2017).
15. Z. Li, Y. Tong, X. Fu, J. Wang, Q. Guo, H. Yu, and X. Bao, "Simultaneous distributed static and dynamic sensing based on ultra-short fiber Bragg gratings," Opt. Express **26**, 17437 (2018).
16. R. Cheng and L. Xia, "Interrogation of weak Bragg grating sensors based on dual-wavelength differential detection," Opt. Lett. **41**, 5254 (2016).
17. H. Wang and Z. Li, "Accurate and fast wavelength demodulation for FBG reflected spectrum using multilayer perceptron (mlp) neural network," in *12th International Conference on Measuring Technology and Mechatronics Automation (ICMTMA)* (2020), p. 265.
18. Y. Wang, J. Gong, D. Y. Wang, B. Dong, W. Bi, and A. Wang, "A quasi-distributed sensing network with time-division-multiplexed fiber Bragg gratings," IEEE Photon. Technol. Lett. **23**, 70 (2010).
19. C. Hu, H. Wen, and W. Bai, "A novel interrogation system for large scale sensing network with identical ultra-weak fiber Bragg gratings," J. Lightwave Technol. **32**, 1406 (2014).
20. L. Ma, C. Ma, Y. Wang, D. Y. Wang, and A. Wang, "High-speed distributed sensing based on ultra weak FBGs and chromatic dispersion," IEEE Photon. Technol. Lett. **28**, 1344 (2016).
21. B. Redding, M. Alam, M. Seifert, and H. Cao, "High-resolution and broadband all-fiber spectrometers," Optica **1**, 175 (2014).
22. Y. Wan, S. Wang, X. Fan, Z. Zhang, and Z. He, "High-resolution wavemeter using Rayleigh speckle obtained by optical time domain reflectometry," Opt. Lett. **45**, 799 (2020).
23. R. K. Gupta, G. D. Bruce, S. J. Powis, and K. Dholakia, "Deep learning enabled laser speckle wavemeter with a high dynamic range," Laser Photonics Rev. **14**, 2000120 (2020).
24. M. J. Murray, A. Davis, C. Kirkendall, and B. Redding, "Speckle-based strain sensing in multimode fiber," Opt. Express **27**, 28494 (2019).
25. P. Healey, "Fading in heterodyne OTDR," Electron. Lett. **20**, 30 (1984).
26. J. W. Goodman, *Speckle Phenomena in Optics: Theory and Applications* (Roberts and Company, 2007).
27. B. Redding, S. M. Popoff, and H. Cao, "All-fiber spectrometer based on speckle pattern reconstruction," Opt. Express **21**, 6584 (2013).
28. T. Hastie, R. Tibshirani, J. H. Friedman, and J. H. Friedman, *The Elements of Statistical Learning: Data Mining, Inference, and Prediction*, Vol. **2** (Springer, 2009).
29. D. P. Kingma and J. Ba, "Adam: a method for stochastic optimization," arXiv:1412.6980 (2014).